

Epitaxial growth and characterization of approx.300-nm-thick AlInN films nearly lattice-matched to c-plane GaN grown on sapphire

Makoto Miyoshi^{1,2*}, Mizuki Yamanaka¹, Takashi Egawa^{1,2}, and Tetsuya Takeuchi³

¹ *Research Center for Nano Devices and Advanced Materials, Nagoya Institute of Technology, Nagoya 466-8555, Japan*

² *Innovation Center for Multi-Business of Nitride Semiconductors, Nagoya Institute of Technology, Nagoya 466-8555, Japan*

³ *Faculty of Science and Technology, Meijo University, Nagoya 468-8502, Japan*

*E-mail: miyoshi.makoto@nitech.ac.jp

AlInN epitaxial films with film thicknesses up to approximately 300 nm were grown nearly lattice-matched to a *c*-plane GaN-on-sapphire template by metalorganic chemical vapor deposition. The AlInN films showed relative good crystal qualities and flat surfaces, despite the existence of surface pits connecting to dislocations in the underlying GaN film. The refractive index derived in this study was in good agreement with a previously reported result in whole visible wavelength. The extinction coefficient spectrum showed a clear absorption edge, and the bandgap energy for AlInN nearly lattice-matched to GaN was determined to be approximately 4.0 eV.

Recently, ternary InAlN alloys are widely utilized as component materials for GaN-based electronic and optical devices¹⁾, such as heterostructure field-effect transistors (HFETs)²⁻⁵⁾, light-emitting diodes (LEDs)⁶⁻⁸⁾, laser diodes (LDs)⁹⁻¹³⁾, photodetectors^{14,15)} and waveguides¹⁶⁾. For optical devices, not only the use as electron-blocking layers^{6,7)}, cladding layers^{11-13,16)} or distributed Bragg reflectors (DBRs)^{8-10,17-21)}, but also the application of thick *m*-plane AlInN films to active light-emitting layers has been proposed^{22,23)}. In addition to their attractive bandgap nature with an extremely wide range from 0.7 eV for InN to 6.2 eV for AlN, the most distinguishing feature of AlInN is to be lattice-matched to GaN. When it comes to visible LDs based on *c*-plane GaN, for example, AlInN alloys seems to be more appropriate as cladding layers than conventional GaN/AlGaN superlattices or single-layer AlGaN films^{24,25)}. That is, regarding cladding layers in LDs, a sufficiently-thick film with a flat surface and a large index contrast to an active layer is required to achieve a high optical confinement factor. In the case of AlGaN-based cladding layers, however, it was difficult to satisfy those conditions at the same time, due to the in-plane tensile strain resulting from lattice-mismatching. In contrast, AlInN with an alloy composition lattice-matched to *c*-plane GaN, an InN molar fraction of approximately 17%, shows a large index contrast in whole visible wavelength¹⁹⁾. Up to now, however, only a few research groups have reported on single-layer AlInN films with thicknesses greater than 100 nm^{12,13,23,26)}. Moreover, two of them^{12,13)} only described the use of AlInN films as a component in GaN LDs, and there is no detailed information on their growth or film qualities. The others^{23,26)} are reports on microstructures of thick AlInN films with non-flat surfaces. In this study, therefore, we attempted to grow thick and flat-surface single-layer AlInN films nearly lattice-matched to *c*-plane GaN by metalorganic chemical vapor deposition (MOCVD) and to characterize them. This research work was conducted to realize a high-quality AlInN cladding layers for high-efficiency/high-power visible GaN LDs.

AlInN films with an alloy composition nearly lattice-matched to GaN were grown by MOCVD on a

GaN-on-sapphire template, which consisted of an MOCVD-grown 2- μm -thick GaN film on a 2-inch-diameter *c*-plane sapphire substrate. For the MOCVD process, trimethyl-aluminum, trimethyl-indium and NH_3 were used as precursors. During AlInN growth, the susceptor temperature and reactor pressure were kept at 830°C and 13.3 kPa, respectively, and the growth rate was adjusted to be approximately 0.6 μm . To estimate the alloy composition, the X-ray diffraction (XRD) ω - 2θ scanning technique was utilized. Further, X-ray rocking curve (XRC) measurement, atomic-force microscopy (AFM) and cross-sectional transmission electron microscopy (TEM) were used for evaluating the film qualities. The film thicknesses, optical constants and energy bandgaps for AlInN films were analytically determined using spectroscopic ellipsometry (SE) measurement.

Figure 1 shows typical XRD ω - 2θ scanning profiles taken around (0002) reflections for samples with AlInN films grown for 4 min, 9 min, and 30 min. For comparison, Fig.1 also shows simulation XRD patterns obtained by assuming lattice-matched $\text{Al}_{0.17}\text{In}_{0.83}\text{N}/\text{GaN}$ structures on sapphire with the AlInN film thicknesses of 40 nm, 90 nm, and 100 nm. As seen in this figure, the experimental and simulation patterns are relatively in good agreement. From this, it was confirmed that the MOCVD-grown AlInN films were in single-phase crystals with alloy compositions and film thicknesses close to the intended structures. In addition, the periodical fringe peaks clearly observed in the XRD profiles probably indicate that abrupt surfaces and interfaces were realized in the AlInN/GaN heteroepitaxial structures. More precisely, the film thicknesses were estimated by analyzing SE measurement results, as described later, and the alloy compositions were determined by applying lattice constants obtained from XRD ω - 2θ measurements to the following equation²⁷⁾.

$$\frac{c - c_0}{c_0} = -2 \frac{C_{13}}{C_{33}} \frac{a - a_0}{a_0}, \quad (1)$$

where C_{13} and C_{33} are the elastic stiffness constants, a_0 and c_0 are the room-temperature lattice constants of

free-standing crystals, and a and c are the measured lattice constants. Here, a_0 and c_0 of AlInN are determined according to Vegard's law^{28,29)} using the following lattice constants³⁰⁾: a_0 is 3.112 Å for AlN and 3.54 Å for InN, and c_0 is 4.982 Å for AlN and 5.705 Å for InN. Further, the elastic constants, C_{13} and C_{33} , were determined by assuming a linear interpolation between AlN and InN based on the following material constants³¹⁾: C_{13} is 94 GPa for AlN and 70 GPa for InN, and C_{33} is 377 GPa for AlN and 205 GPa for InN. The determined InN molar fractions x_{In} in AlInN and film thicknesses t are noted in Fig.1.

The crystal quality of the AlInN films was evaluated using XRC measurement, surface AFM observation and cross-sectional TEM observation. Figures 2(a) and 2(b) show XRC profiles taken for symmetric (0002) and asymmetric ($10\bar{1}2$) reflections, respectively. Full widths at half maximum (FWHMs) in XRCs for AlInN films showed relative good values as around 200 s and 300 s for the (0002) and ($10\bar{1}2$) reflections in all samples. These XRC-FWHM values are close to those for the underlying GaN films, as shown in Fig. 2. This probably indicates that the crystal mosaicity in the AlInN films is strongly dependent on the GaN films. Figures 3(a), 3(b) and 3(c) show surface AFM images and corresponding root-mean-square (RMS) roughness values for samples grown for 4 min, 9 min and 30 min, respectively. The observation results revealed that the AlInN surfaces consisted of flat areas and a certain number of pits. Further, it was obvious that these pits increased in size with the increase in AlInN film thickness. Although the measured RMS values were not as small as an atomic order level, they were construed to be rather good results considering the influence of the pits on the RMS estimate. To understand the origin of the pits, cross-sectional TEM observation was carried out. Here, the focused-ion-beam milling technique was adopted for the sample thinning so as to directly observe a cross-section just beneath the surface pits. Figures 4(a) and 4(b) show cross-sectional TEM dark-field images taken with g -vectors parallel to the [0002] and [$11\bar{2}0$] directions, respectively, for the sample grown for 30 min. As seen in the TEM images, it was found that the pits formed on the AlInN surfaces resulted

from threading dislocations in the underlying GaN films. In more detail, it was also confirmed that a few of the observed dislocations disappeared from the image with the g -vector in the [0002] direction but did not disappear from the image with that in the [11 $\bar{2}$ 0] direction. From this, at least in this view field, the origin of the surface pits was considered to be the pure-edge and edge/screw-mixed type dislocations.

By using the SE analyses, we can obtain not only the film thicknesses for epitaxial films but also their optical constants as well as energy bandgaps. The SE measurement yields two parameters, the amplitude ratio Ψ and the phase parameter Δ in the complex reflectance ratio $r_p/r_s = \tan \Psi \cdot e^{i\Delta}$, where the r_p and r_s are the complex field reflectance for s - and p -polarized light, respectively. Figures 5(a) and 5(b) show the measured waveforms of Ψ and Δ , respectively, for an AlInN film grown for 30 min on a GaN-on-sapphire template. In these figures, the oscillation observed in a wavelength range shorter than 365 nm corresponds to the reflection from the AlInN film, and the oscillation at longer wavelength than that includes information from both the AlInN and GaN films. The film thicknesses and the optical constants, the refractive index n and extinction coefficient k , were derived by fitting the Tauc-Lorentz oscillator model³²⁾ to the measured waveforms. As seen in Figs. 5(a) and 5(b) it was confirmed that the model fitting was conducted well. Figures 6(a) and 6(b) show the derived n and k , respectively, as a function of the incidence wavelength. For comparison, past research results obtained for an Al_{0.825}In_{0.175}N film on GaN¹⁹⁾ are also plotted in these figures. From Fig. 6(a), it is obvious that the derived n was well consistent with that given in the previous report¹⁹⁾ in the whole visible wavelength range. As seen in Fig. 6(b), on the other hand, the spectrum of the k showed a somewhat abrupt curve compared to that of the reported result¹⁹⁾. This may indicate that the AlInN films grown in this study have superior crystal quality. The bandgap energy E_g can be derived from the extended Tauc formula $(\alpha E)^r \cong (E - E_g)^{19}$. In this equation, an exponent $r = 2$ is reported to be appropriate for considering direct-transition semiconductors^{19,33)}, and the light absorption coefficient α is represented by $\alpha = 4\pi k/\lambda$ using the derived k and the incidence

wavelength λ . Thus, the E_g is determined from the intersection of the tangent of $(\alpha E)^2$ with the energy axis. Figure 7 plots the $(\alpha E)^2$ as a function of photon energy. As a result of the sharp extinction coefficient curve seen in Fig. 6(b), the spectrum in Fig. 7 also showed an abrupt absorption edge compared to the previously reported result¹⁹⁾. Eventually, the E_g of the $\text{Al}_{0.836}\text{In}_{0.164}\text{N}$ film nearly lattice-matched to GaN was determined to be 4.02 eV in this study.

In conclusion, single-layer AlInN epitaxial films with film thicknesses up to approximately 300 nm were grown nearly lattice-matched to a *c*-plane GaN-on-sapphire template by MOCVD. The XRC-FWHMs for AlInN films were approximately 200 s and 300 s for (0002) and (10 $\bar{1}$ 2) reflections, respectively. This probably indicates that the crystal mosaicity in the AlInN films is strongly dependent on the underlying GaN films. The AFM observation revealed that the sample surfaces consisted of flat areas and a certain number of pits and that those pits were enlarged with an increase in the AlInN film thickness. The RMS surface roughness was measured to be approximately 1.8 nm for the sample with an AlInN film thickness of approximately 300 nm. The cross-sectional TEM observation revealed that the surface pits were caused by the threading dislocations in the underlying GaN films. The optical constants of an AlInN film were estimated by SE measurement. The refractive index was confirmed to be well consistent with that in the previous report. The extinction coefficient showed a somewhat sharp absorption edge compared to the previous report. By using this result, the bandgap energy of the AlInN film nearly lattice-matched to GaN was estimated to be 4.02 eV.

Acknowledgement: This work was partially supported by the MEXT “Program for research and development of next-generation semiconductor to realize energy-saving society”.

References

- 1) R. Butté, J.-F. Carlin *et al.*, J. Phys. D: Appl. Phys. **40**, 6238 (2007).
- 2) J. Kuzmik, A. Kostopoulos, G. Konstantinidis, J.-F. Carlin, A. Georgakilas, and D. Pogany, IEEE Trans. Electron Devices **53**, 422, (2006).
- 3) F. Medjdoub, J.-F. Carlin, M. Gonschorek, E. Feltin, M.A. Py, D. Ducatteau, C. Gaquière, N. Grandjean, and E. Kohn, IEDM Tech. Dig., 2006, p.1.
- 4) M. Miyoshi, Y. Kuraoka, M. Tanaka, and T. Egawa, Appl. Phys. Express **1**, 081102 (2008).
- 5) M. Miyoshi, T. Tsutsumi, G. Nishino, Y. Miyachi, M. Okada, and J. J. Freedman, and T. Egawa, J. Vac. Sci. Technol. B **34**, 050602 (2016).
- 6) S. Choi, H. J. Kim, S-S. Kim, J. Liu, J. Kim, J-H. Ryou, R. D. Dupuis, A. M. Fischer, and F. A. Ponce, Appl. Phys. Lett. **96**, 221105 (2010).
- 7) Y-Y. Zhang, X-L. Zhu, Y-A. Yin, and J. Ma, IEEE Electron Device Lett. **33**, 994 (2012).
- 8) H. Isihikawa, T. Jimbo, and T. Egawa, Phys. Stat. Sol. C **5**, 2086 (2008).
- 9) K. Ikeyama, Y. Kozuka, K. Matsui, S. Yoshida, T. Akagi, Y. Akatsuka, N. Koide, T. Takeuchi, S. Kamiyama, M. Iwaya, and I. Akasaki, Appl. Phys. Express **9**, 102101 (2016).
- 10) G. Cosendey, A. Castiglia, G. Rossbach, J.-F. Carlin, and N. Grandjean. Appl. Phys. Lett. **101**, 151113 (2012)
- 11) H. P. D. Schenk, M. Nemoz, M. Korytov, P. Vennéguès, A. D. Dräger, and A. Hangleiter, Appl. Phys. Lett. **93**, 081116 (2008).
- 12) T. Frost, A. Hazari, A. Aiello, M. Z. Baten, L. Yan, J. Mirecki-Millunchick, and P. Bhattacharya, Jpn. J. Appl. Phys. **55**, 032101 (2016).
- 13) A. Castiglia, E. Feltin, J. Dorsaz, G. Cosendey, J.-F. Carlin, R. Butté, and N. Grandjean, Electronics

- Lett. **44**, 521 (2008).
- 14) S. Senda, H. Jiang, and T. Egawa, Appl. Phys. Lett. **92**, 203507 (2008).
 - 15) L. Li, D. Hosomi, Y. Miyachi, T. Hamada, M. Miyoshi, and T. Egawa, Appl. Phys. Lett. **111**, 102106 (2017).
 - 16) A. Lupu, F. H. Julien, S. Golka, G. Pozzovivo, G. Strasser, E. Baumann, F. Giorgetta, D. Hofstetter, S. Nicolay, M. Mosca, E. Felton, J.-F. Carlin, and N. Grandjean, IEEE Photonics Technol. Lett. **20**, 102 (2008).
 - 17) J.-F. Carlin, and M. Illegems, Appl. Phys. Lett. **83**, 668 (2003).
 - 18) J.-F. Carlin, C. Zellweger, J. Dorsaz, S. Nicolay, G. Christmann, E. Felton, R. Butté, and N. Grandjean, Phys. Stat. Sol. B **242**, 2326 (2005).
 - 19) T. Aschenbrenner, H. Dartsch, C. Kruse, M. Anastasescu, M. Stoica, M. Gartner, A. Pretorius, A. Rosenauer, T. Wagner, and D. Hommel, J. Appl. Phys. **108**, 063533 (2010).
 - 20) Y. Kozuka, K. Ikeyama, T. Yasuda, T. Takeuchi, S. Kamiyama, M. Iwaya, and I. Akasaki, 2015 MRS Proc. 1736 mrsf14-1736-t13-08.
 - 21) S. Yoshida, K. Ikeyama, T. Yasuda, T. Furuta, T. Takeuchi, M. Iwaya, S. Kamiyama, and I. Akasaki, Jpn. J. Appl. Phys. **55**, 05FD10 (2016).
 - 22) S. F. Chichibu, K. Hazu, K. Furusawa, Y. Ishikawa, T. Onuma, T. Ohtomo, H. Ikeda, and K. Fujito, J. Appl. Phys. **116**, 213501 (2014).
 - 23) S. F. Chichibu, K. Kojima, A. Uedono, and Y. Sato, Adv. Mater. **29**, 1603644 (2017).
 - 24) S. Nakamura, Solid State Commun. **102**, 237 (1997).
 - 25) S. Nakamura, M. Senoh, S. Nagahama, N. Iwasa, T. Yamada, T. Matsushita, H. Kiyoku, Y. Sugimoto, T. Kozaki, H. Umemoto, M. Sano, K. Chocho, J. Cryst. Growth 189–190, 820 (1998).

- 26) S. Kret, A Wolska, M. T. Klepka, A. Letrouit, F. Ivaldi, A. Szczepańska, J-F. Carlin, N. A. K. Kaufmann, and N. Grandjean, *J. Phys.: Conf. Ser.* **326**, 012013 (2011).
- 27) T. Takeuchi, H. Takeuchi, S. Sota, H. Sakai, H. Amano, and I. Akasaki, *Jpn. J. Appl. Phys.* **36**, L177 (1997).
- 28) R. R. Pelá, C. Caetano, M. Marques, L. G. Ferreira, J. Furthmüller, and L. K. Teles, *Appl. Phys. Lett.* **98**, 151907 (2011).
- 29) J. Dion, Q. Fareed, B. Zhang, and A. Khan, *J. Electron. Mater.* **40**, 377 (2011).
- 30) M. Shur, M. Shatalov, A. Dobrinsky, and R. Gaska, in *GaN and ZnO-Based Materials and Devices*, ed. S. Pearton (Springer, Heidelberg, 2012) Springer Series in Materials Science, Vol. 156, p. 83.
- 31) F. Bernardini, V. Fiorentini, and D. Vanderbilt, *Phys. Rev. B* **63**, 193201 (2001).
- 32) J. G. E. Jellison and F. A. Modine, *Appl. Phys. Lett.* **69**, 371 (1996).
- 33) J. Tauc, R. Grigorovici, and A. Vancu, *Phys. Stat. Solidi B* **15**, 627 (1966).

Figure captions

Fig. 1. (Color online) Typical XRD ω - 2θ profiles taken around (0002) reflections for AlInN/GaN heteroepitaxial films grown, from bottom to top, for 4 min, 9 min and 30 min (blue lines), and the simulation profiles obtained by assuming lattice-matched $\text{Al}_{0.17}\text{In}_{0.83}\text{N}/\text{GaN}$ structures on sapphire with the AlInN film thicknesses of 40 nm, 90 nm and 300 nm (red lines). The text notes show the InN molar fractions x_{In} in AlInN alloys and their film thicknesses t . Here, the experimental values for x_{In} and t were obtained from their lattice constants and from the SE measurement results, respectively.

Fig. 2. (Color online) Typical XRC profiles taken for (a) symmetric (0002) and (b) asymmetric ($10\bar{1}2$) reflections for MOCVD-grown AlInN films and the underlying GaN films.

Fig. 3. (Color online) Surface AFM images for AlInN films grown for (a) 4 min, (b) 9 min and (c) 30 min on GaN-on-sapphire templates by MOCVD.

Fig. 4. Cross-sectional TEM dark-field images taken with g -vectors parallel to the (a) [0002] and (b) [$11\bar{2}0$] directions for an AlInN film grown for 30 min on a GaN-on-sapphire template.

Fig. 5. (Color online) Waveforms of (a) Ψ and (b) Δ obtained at different incidence angles of 65° , 75° and 85° by SE measurement for an AlInN film grown for 30 min on a GaN-on-sapphire template (blue lines), and the fitted waveforms based on the Tauc-Lorentz oscillator model (red lines).

Fig. 6. (Color online) Spectra of (a) refractive index n and (b) extinction coefficient k determined for the AlInN and GaN films. For comparison, past research results²¹⁾ are also plotted.

Fig. 7. (Color online) Absorption spectra determined for the AlInN and GaN films. For comparison, a past research result for an AlInN film²¹⁾ is also plotted.

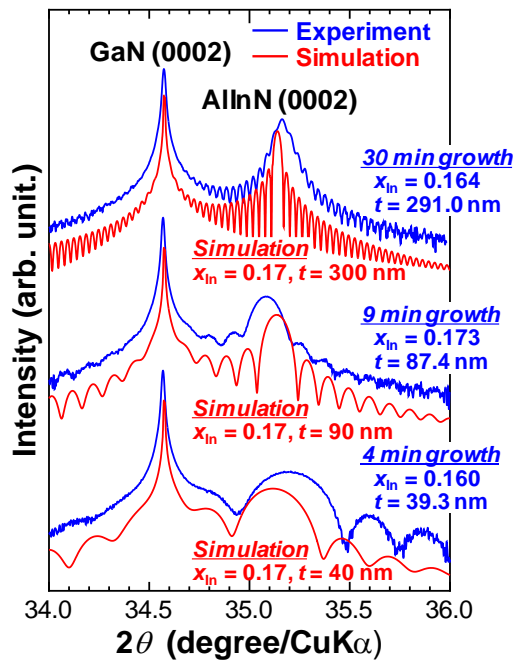


Fig. 1

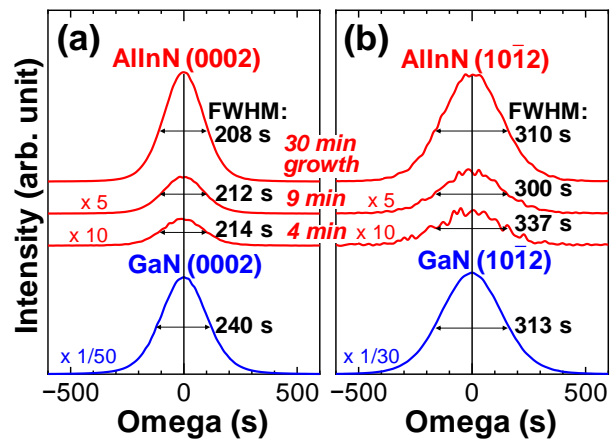


Fig. 2

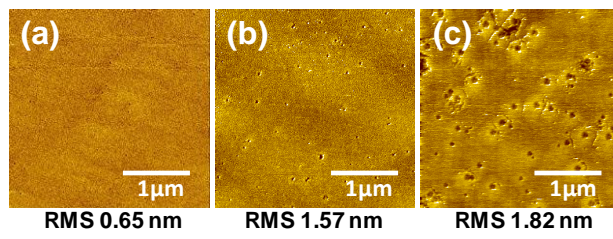


Fig. 3

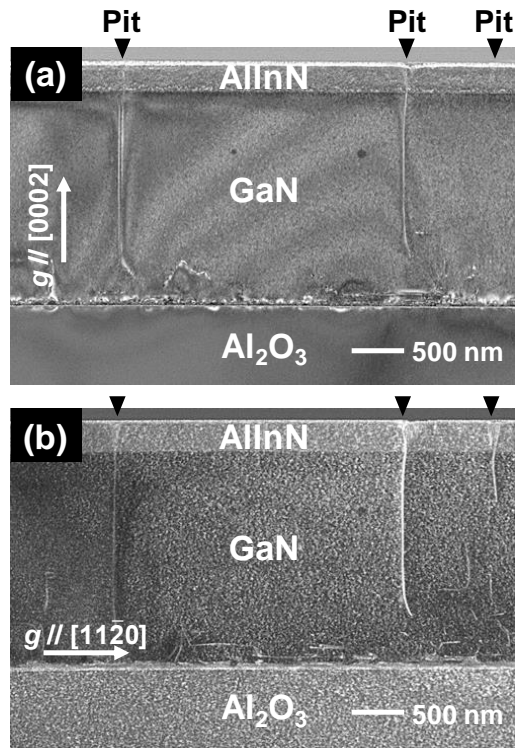


Fig. 4

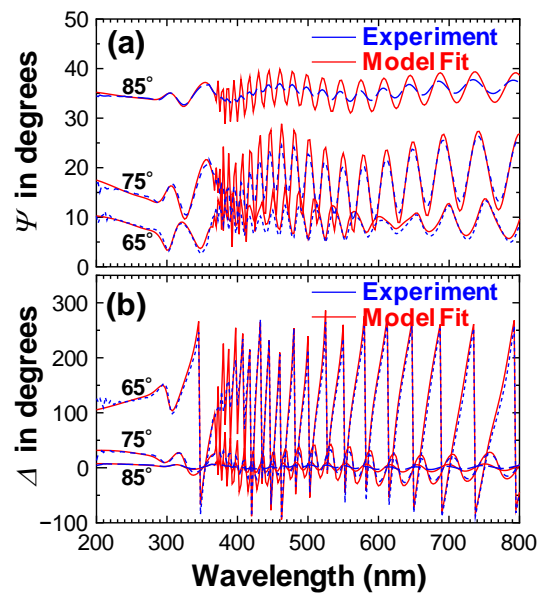


Fig. 5

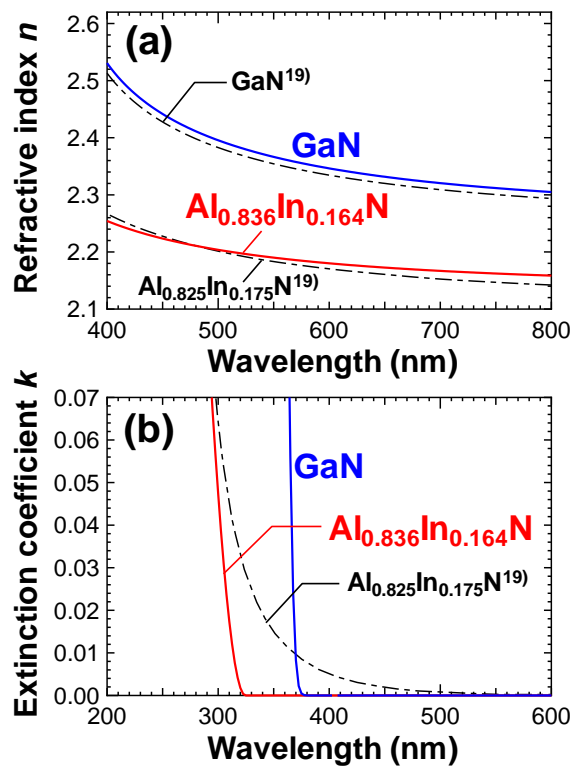


Fig. 6

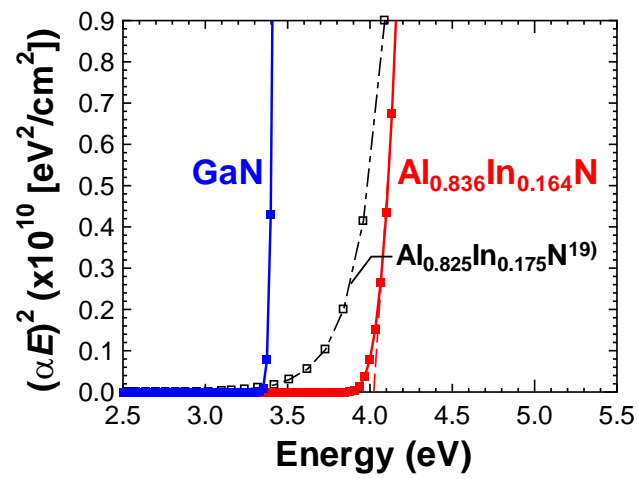


Fig. 7